Landau theory for the phase diagram of multiferroic $Mn_{1-x}(Fe,Zn,Mg)_xWO_4$

Shlomi Matityahu,[1] Amnon Aharony,[1,2,*] and Ora Entin-Wohlman[1,2,†]
[1]*Department of Physics, Ben-Gurion University, Beer Sheva 84105, Israel*
[2]*Ilse Katz Center for Meso- and Nano-Scale Science and Technology, Ben-Gurion University, Beer Sheva 84105, Israel*
(Received 2 March 2012; revised manuscript received 5 April 2012; published 8 May 2012)

We present a theoretical analysis of the temperature magnetic field concentration phase diagram of the multiferroic $Mn_{1-x}M_xWO_4$ (M = Fe, Zn, Mg), which exhibits three ordered phases, with collinear and noncollinear incommensurate and with a commensurate magnetic order. The middle phase is also ferroelectric. The analysis uses a semiphenomenological Landau theory based on a Heisenberg Hamiltonian with a single-ion anisotropy. With a small number of adjustable parameters, the Landau theory gives an excellent fit to all three transition lines as well as the magnetic and the ferroelectric order parameters. The fit of the magnetic and ferroelectric order parameters is further improved by including the effect of fluctuations near the transitions. We demonstrate the highly frustrated nature of these materials and suggest a simple explanation for the dramatic effects of doping with different magnetic ions at the Mn sites. The model enables an examination of different sets of exchange couplings that were proposed by a number of groups. Small discrepancies are probably a consequence of small errors in the experimental magnetic parameters. In addition, using the Ginzburg criterion, we estimate the temperature range in which fluctuations of the order parameters become important.

DOI: 10.1103/PhysRevB.85.174408 PACS number(s): 75.40.−s, 75.10.Jm, 77.80.B−, 75.85.+t

I. INTRODUCTION

Type-II magnetoelectric multiferroics are materials which exhibit coexistence between certain types of long-range magnetic order and a ferroelectric order. These materials are usually characterized by a strong magnetoelectric coupling between their electric and magnetic degrees of freedom. The magnetoelectric effect enables the control of the electric polarization by a magnetic field, or the control of the magnetization by an electric field. The study of magnetoelectric multiferroics is thus of great interest in condensed matter physics, both from basic research and technological applications points of view.[1–4] In recent years, the interest in this field has grown after the discovery of new materials with a large magnetoelectric effect, such as $TbMnO_3$,[5] $TbMn_2O_5$,[6] $Ni_3V_2O_8$,[7] $CuFeO_2$,[8] and $CoCr_2O_4$.[9] In those oxides, ferroelectricity appears in conjunction with a noncollinear spiral magnetic phase, which breaks spatial inversion symmetry, and therefore allows the appearance of an electric polarization.

There are two different approaches to the theoretical treatment of such noncollinear magnetoelectric multiferroics. One approach is based on first-principles calculations using the density functional theory (DFT).[10] The second approach constructs a model Hamiltonian dictated by symmetry considerations.[7,11,12] Different mechanisms for the magnetoelectric coupling can then be suggested.[1,13–15] In this paper, we develop a semiphenomenological model for describing the magnetic phase transitions of $Mn_{1-x}M_xWO_4$ (M = Fe, Zn, Mg) and the induced ferroelectric polarization. The model is semiphenomenological in the sense that some of the parameters can be deduced from existing experimental data, while the others are purely phenomenological. The multiferroic $MnWO_4$ is a natural choice for such an approach, due to the vast experimental data that exists in the literature.

$MnWO_4$ crystallizes in the wolframite structure, which belongs to the monoclinic space group $P2/c$ with $\beta \approx 91^\circ$. The unit cell includes two magnetic Mn^{2+} ions with spin $S = 5/2$ and orbital angular momentum $L = 0$ at positions $\boldsymbol{\tau}_1 = (0.5, y, 0.25)$ and $\boldsymbol{\tau}_2 = (0.5, 1-y, 0.75)$ (in units of the primitive lattice vectors) with $y = 0.685$.[16] In zero magnetic field, $MnWO_4$ undergoes three successive phase transitions at temperatures $T_{N3} \approx 13.5$ K, $T_{N2} \approx 12.3$–12.7 K, and $T_{N1} \approx 7$–8 K to phases which are called AF3, AF2, and AF1, respectively.[16–18] According to neutron diffraction experiments,[16] AF3 is an incommensurate (IC) antiferromagnetic phase with a collinear sinusoidal structure, AF2 is an incommensurate antiferromagnetic phase with an elliptical-spiral structure, and AF1 is a commensurate (C) antiferromagnetic phase with a collinear $\uparrow\uparrow\downarrow\downarrow$ structure. The propagation vectors are $\boldsymbol{q}_{IC} = (-0.214, 0.5, 0.457)$ (in units of the primitive reciprocal lattice vectors) for AF2 and AF3, and $\boldsymbol{q}_{C1,2} = (\pm 0.25, 0.5, 0.5)$ for AF1. In AF3 and AF1, the magnetic moments of the Mn^{2+} ions align along the easy axis of magnetization, which lies in the ac plane and forms an angle of $\approx 35^\circ$–37° with the a axis. Different studies[17,18] reveal that a ferroelectric polarization, which is oriented along the b axis, develops in the AF2 phase.

As opposed to $MnWO_4$, other isomorphic wolframite structures such as $FeWO_4$, $CoWO_4$, and $NiWO_4$ show only a single magnetic phase transition to a simple commensurate antiferromagnetic phase with the propagation vector $\boldsymbol{q} = (0.5, 0, 0)$.[19] Those observations suggest that unlike the isomorphic structures, $MnWO_4$ constitutes a highly frustrated system with complex competing interactions. The competition between the different interactions manifests itself in the sensitivity of the phase diagram to doping with different transition-metal ions at the Mn sites. It turns out that a small Fe concentration suppresses the ferroelectric phase AF2 and expands the stabilization range of AF3 and AF1.[20–22] In contrast to Fe doping, it has been reported[23] that a small Co concentration stabilizes the ferroelectric phase at the expense of the AF1 phase. A quantitative and microscopic understanding of the effect of Fe and Co doping on the multiferroic properties and the phase diagram of $MnWO_4$ is quite complicated since the exchange couplings of the M-M

and M-Mn (M = Fe, Co) interactions as well as the anisotropy parameters are not known. In order to overcome some of these problems, a much simpler magnetic system has been achieved by the partial substitution of Mn ions by the nonmagnetic ions Zn^{2+} and Mg^{2+}.[24,25] Those studies reveal that the AF1 phase is strongly suppressed as a result of magnetic ions dilution by nonmagnetic substituents.

The frustrated nature of $MnWO_4$ was demonstrated by Ehrenberg *et al.*[26] Using inelastic neutron scattering, they extracted nine exchange couplings $J_1 - J_9$ for the superexchange interactions among the Mn ions. Later, Tian *et al.*[27] proposed different values for the nine exchange couplings based on DFT calculations. Those values depend on an unknown onsite repulsion energy. Moreover, the authors have noted that generally DFT calculations tend to overestimate the magnitude of exchange interactions.[27] Recently, the experimental data have been expanded.[28] In that study, Ye *et al.* suggested some corrections for the values of the exchange couplings, and included two additional ones, J_{10} and J_{11}. The two sets of experimental exchange couplings are summarized in Table I. Since we suspect that in the definitions of the exchange term in Ref. 26 each term was counted twice, we also added another line with the exchange couplings of that work multiplied by a factor of 2.[29] The model we describe may help to compare these different sets of exchange couplings by examining their consistency with different experimental observations.

The outline of the paper is as follows: In Sec. II, we define the model. In Sec. III, the results of the model are derived. In Sec. IV, the model parameters are fitted by comparing their results with different experimental observations. Here, we compare the two sets of experimental exchange couplings with the fitted parameters. In Sec. V, the Ginzburg criterion is applied to the specific case of the multiferroic $MnWO_4$ in order to examine whether the mean-field-theory approach is valid. We conclude in Sec. VI with a brief summary.

II. THE MODEL

In this section, we develop the semiphenomenological model. The spin Hamiltonian consists of a Heisenberg term with a single-ion anisotropy, which favors an easy axis in the *ac* plane. According to experiments, the spin component along the hard axis in the *ac* plane does not order in any of the phases. Furthermore, the transitions are almost not influenced by an external magnetic field along the hard axis. Hence, we omit the hard axis component from the calculations and write the spin as $\boldsymbol{S}(\boldsymbol{R}+\boldsymbol{\tau}) = S_x(\boldsymbol{R}+\boldsymbol{\tau})\hat{\mathbf{x}} + S_b(\boldsymbol{R}+\boldsymbol{\tau})\hat{\mathbf{b}}$, where x denotes the easy axis in the *ac* plane and b denotes the axis perpendicular to the *ac* plane. Here, $\boldsymbol{S}(\boldsymbol{R}+\boldsymbol{\tau})$ is the thermal average of the dimensionless classical spin at position $\boldsymbol{R}+\boldsymbol{\tau}$, where $\boldsymbol{R}$ is a lattice vector and $\boldsymbol{\tau}$ is one of the two basis vectors $\boldsymbol{\tau}_1, \boldsymbol{\tau}_2$ in the unit cell, indicating the locations of the Mn^{2+} ions. We study the following Hamiltonian:

$$H_{\mathrm{mag}} = -\frac{1}{2}\sum_{\boldsymbol{R},\boldsymbol{R}'}\sum_{\boldsymbol{\tau},\boldsymbol{\tau}'=\boldsymbol{\tau}_1,\boldsymbol{\tau}_2} J(\boldsymbol{R}+\boldsymbol{\tau},\boldsymbol{R}'+\boldsymbol{\tau}') \times \boldsymbol{S}(\boldsymbol{R}+\boldsymbol{\tau})\cdot\boldsymbol{S}(\boldsymbol{R}'+\boldsymbol{\tau}') - \frac{1}{2}D\sum_{\boldsymbol{R}}\sum_{\boldsymbol{\tau}=\boldsymbol{\tau}_1,\boldsymbol{\tau}_2} {S_x}^2(\boldsymbol{R}+\boldsymbol{\tau}). \quad (1)$$

TABLE I. Superexchange couplings for the Mn^{2+} ion at $\boldsymbol{\tau}_1 = (0.5, y, 0.25)$ according to different inelastic neutron scattering studies. We denote $z = 1 - y$, $w = 2 - y$, and $u = 1 + y$. The values are presented in units of k_B K (Ref. 30). The third line, denoted as Ref. 26*, is the couplings of Ref. 26 multiplied by a factor of 2.

	J_1	J_2	J_3	J_4	J_5	J_6	J_7	J_8	J_9	J_{10}	J_{11}	D
Neighbors	$(\frac{1}{2},z,\frac{3}{4})$	$(\frac{1}{2},w,\frac{3}{4})$	$(\frac{3}{2},y,\frac{1}{4})$	$(\frac{1}{2},y,\frac{5}{4})$	$(\frac{1}{2},u,\frac{1}{4})$	$(\frac{3}{2},z,\frac{3}{4})$	$(-\frac{1}{2},z,\frac{3}{4})$	$(\frac{3}{2},w,\frac{3}{4})$	$(-\frac{1}{2},w,\frac{3}{4})$	$(\frac{3}{2},y,\frac{5}{4})$	$(\frac{3}{2},y,-\frac{3}{4})$	
	$(\frac{1}{2},z,-\frac{1}{4})$	$(\frac{1}{2},w,-\frac{1}{4})$	$(-\frac{1}{2},y,\frac{1}{4})$	$(\frac{1}{2},y,-\frac{3}{4})$	$(\frac{1}{2},-z,\frac{1}{4})$	$(-\frac{1}{2},z,-\frac{1}{4})$	$(\frac{3}{2},z,-\frac{1}{4})$	$(\frac{3}{2},w,-\frac{1}{4})$	$(\frac{3}{2},w,-\frac{1}{4})$	$(-\frac{1}{2},y,-\frac{3}{4})$	$(-\frac{1}{2},y,\frac{5}{4})$	
Ref. 26	−0.195	−0.135	−0.423	0.414	0.021	−0.509	0.023	0.491	−1.273			0.568
Ref. 26*	−0.39	−0.27	−0.846	0.828	0.042	−1.018	0.046	0.982	−2.546			0.568
Ref. 28	−1.95(1)	−0.18(1)	−1.48(1)	−1.21(1)	0.23(1)	−1.99(1)	−0.56(1)	0.09(1)	−1.21(1)	−0.7(1)	0.09(1)	0.84(1)

Here, $J(\boldsymbol{R}+\boldsymbol{\tau},\boldsymbol{R}'+\boldsymbol{\tau}')$ is the superexchange interaction energy which couples the spins at $\boldsymbol{R}+\boldsymbol{\tau}$ and $\boldsymbol{R}'+\boldsymbol{\tau}'$, and D is a positive single-ion anisotropy energy. To find an expression for the magnetic free energy of the system, we expand the entropy in the spin components up to the fourth order

$$TS = -\frac{1}{2}aT\sum_{\boldsymbol{R}}\sum_{\boldsymbol{\tau}=\boldsymbol{\tau}_1,\boldsymbol{\tau}_2}\boldsymbol{S}^2(\boldsymbol{R}+\boldsymbol{\tau}) - b\sum_{\boldsymbol{R}}\sum_{\boldsymbol{\tau}=\boldsymbol{\tau}_1,\boldsymbol{\tau}_2}\boldsymbol{S}^4(\boldsymbol{R}+\boldsymbol{\tau}), \tag{2}$$

where a and b are positive parameters, and T is the temperature. Equation (2) gives the entropy relative to the high-temperature paramagnetic phase (denoted by P) and thus the expression is negative. Combining Eqs. (1) and (2), we obtain the magnetic free energy

$$F_{\mathrm{mag}} = \frac{1}{2}\sum_{\boldsymbol{R},\boldsymbol{R}'}\sum_{\boldsymbol{\tau},\boldsymbol{\tau}'=\boldsymbol{\tau}_1,\boldsymbol{\tau}_2}\sum_{\alpha,\beta=1}^{2}\chi^{-1}_{\alpha\beta}(\boldsymbol{R}+\boldsymbol{\tau},\boldsymbol{R}'+\boldsymbol{\tau}') \times S_\alpha(\boldsymbol{R}+\boldsymbol{\tau})S_\beta(\boldsymbol{R}'+\boldsymbol{\tau}') + b\sum_{\boldsymbol{R}}\sum_{\boldsymbol{\tau}=\boldsymbol{\tau}_1,\boldsymbol{\tau}_2}\boldsymbol{S}^4(\boldsymbol{R}+\boldsymbol{\tau}), \tag{3}$$

where the 4×4 inverse susceptibility matrix is block diagonal:

$$\chi^{-1}_{\alpha\beta}(\boldsymbol{R}+\boldsymbol{\tau},\boldsymbol{R}'+\boldsymbol{\tau}') = [(aT-D_\alpha)\delta_{\boldsymbol{R},\boldsymbol{R}'}\delta_{\tau,\tau'} - J(\boldsymbol{R}+\boldsymbol{\tau},\boldsymbol{R}'+\boldsymbol{\tau}')]\delta_{\alpha,\beta}, \tag{4}$$

with $D_1 = D_x = D$ and $D_2 = D_b = 0$. In the following, we exploit the Fourier transforms of the spin components

$$S_\alpha(\boldsymbol{q},\boldsymbol{\tau}) = \frac{1}{N}\sum_{\boldsymbol{R}}S_\alpha(\boldsymbol{R}+\boldsymbol{\tau})e^{i\boldsymbol{q}\cdot(\boldsymbol{R}+\boldsymbol{\tau})},$$
$$S_\alpha(\boldsymbol{R}+\boldsymbol{\tau}) = \sum_{\boldsymbol{q}}S_\alpha(\boldsymbol{q},\boldsymbol{\tau})e^{-i\boldsymbol{q}\cdot(\boldsymbol{R}+\boldsymbol{\tau})}. \tag{5}$$

Here, $\boldsymbol{q}$ is in the first Brillouin zone and N is the number of unit cells. In terms of the Fourier transform, the magnetic free energy per unit cell, $f_{\mathrm{mag}} \equiv F_{\mathrm{mag}}/N$, is

$$f_{\mathrm{mag}} = \frac{1}{2}\sum_{\boldsymbol{\tau},\boldsymbol{\tau}'=\boldsymbol{\tau}_1,\boldsymbol{\tau}_2}\sum_{\alpha,\beta=1}^{2}\sum_{\boldsymbol{q}}\chi^{-1}_{\alpha\beta}(\boldsymbol{q};\boldsymbol{\tau},\boldsymbol{\tau}')S_\alpha{}^*(\boldsymbol{q},\boldsymbol{\tau})S_\beta(\boldsymbol{q},\boldsymbol{\tau}') + b\sum_{\boldsymbol{G}}\sum_{\boldsymbol{\tau}=\boldsymbol{\tau}_1,\boldsymbol{\tau}_2}\sum_{\boldsymbol{q}_1,\boldsymbol{q}_2,\boldsymbol{q}_3,\boldsymbol{q}_4}e^{-i\boldsymbol{G}\cdot\boldsymbol{\tau}}[S_x(\boldsymbol{q}_1,\boldsymbol{\tau})S_x(\boldsymbol{q}_2,\boldsymbol{\tau})S_x(\boldsymbol{q}_3,\boldsymbol{\tau})S_x(\boldsymbol{q}_4,\boldsymbol{\tau})$$
$$+ S_b(\boldsymbol{q}_1,\boldsymbol{\tau})S_b(\boldsymbol{q}_2,\boldsymbol{\tau})S_b(\boldsymbol{q}_3,\boldsymbol{\tau})S_b(\boldsymbol{q}_4,\boldsymbol{\tau}) + 2S_x(\boldsymbol{q}_1,\boldsymbol{\tau})S_x(\boldsymbol{q}_2,\boldsymbol{\tau})S_b(\boldsymbol{q}_3,\boldsymbol{\tau})S_b(\boldsymbol{q}_4,\boldsymbol{\tau})]\delta(\boldsymbol{q}_1+\boldsymbol{q}_2+\boldsymbol{q}_3+\boldsymbol{q}_4-\boldsymbol{G}), \tag{6}$$

where $\boldsymbol{G}$ is a reciprocal lattice vector and the Fourier transform of the inverse susceptibility matrix is given by the block-diagonal Hermitian matrix

$$\chi^{-1}_{\alpha\beta}(\boldsymbol{q};\boldsymbol{\tau},\boldsymbol{\tau}') = [(aT-D_\alpha)\delta_{\boldsymbol{\tau},\boldsymbol{\tau}'} - J(\boldsymbol{q};\boldsymbol{\tau},\boldsymbol{\tau}')]\delta_{\alpha,\beta}, \tag{7}$$

with $J(\boldsymbol{q};\boldsymbol{\tau},\boldsymbol{\tau}')$ being the Fourier transform of the 2×2 matrix $J(\boldsymbol{R}+\boldsymbol{\tau},\boldsymbol{R}'+\boldsymbol{\tau}')$

$$J(\boldsymbol{q};\boldsymbol{\tau},\boldsymbol{\tau}') = \sum_{\boldsymbol{R}}J(\boldsymbol{\tau},\boldsymbol{R}+\boldsymbol{\tau}')e^{-i\boldsymbol{q}\cdot(\boldsymbol{R}+\boldsymbol{\tau}'-\boldsymbol{\tau})}. \tag{8}$$

In the last expression, the sum is over all lattice vectors $\boldsymbol{R}$. The four eigenvalues of the matrix (7) are

$$\zeta_{\pm,x}(\boldsymbol{q},T) = aT - D - \lambda_\pm(\boldsymbol{q}),$$
$$\zeta_{\pm,b}(\boldsymbol{q},T) = aT - \lambda_\pm(\boldsymbol{q}), \tag{9}$$

and the corresponding eigenvectors are

$$\boldsymbol{S}_{\pm,x}(\boldsymbol{q}) = \frac{1}{\sqrt{2}}\begin{pmatrix}1\\ \pm e^{-i\phi(\boldsymbol{q})}\\ 0\\ 0\end{pmatrix}, \quad \boldsymbol{S}_{\pm,b}(\boldsymbol{q}) = \frac{1}{\sqrt{2}}\begin{pmatrix}0\\ 0\\ 1\\ \pm e^{-i\phi(\boldsymbol{q})}\end{pmatrix}. \tag{10}$$

Here, $\lambda_\pm$ are the two eigenvalues of the matrix (8) and $\phi(\boldsymbol{q})$ is the phase of $J(\boldsymbol{q};1,2)$. Assuming 11 exchange couplings as in Ref. 28, these two eigenvalues are given by

$$\lambda_\pm(\boldsymbol{q}) = \pm 2\sqrt{{\Lambda_2}^2(\boldsymbol{q}) + {\Lambda_3}^2(\boldsymbol{q}) + 2\cos(2\pi q_b)\Lambda_2(\boldsymbol{q})\Lambda_3(\boldsymbol{q})} + 2\Lambda_1(\boldsymbol{q}), \tag{11}$$

with the following definitions:

$$\Lambda_1(\boldsymbol{q}) = J_3\cos(2\pi q_a) + J_4\cos(2\pi q_c) + J_5\cos(2\pi q_b) + J_{10}\cos[2\pi(q_a+q_c)] + J_{11}\cos[2\pi(q_a-q_c)],$$
$$\Lambda_2(\boldsymbol{q}) = J_1\cos(\pi q_c) + J_6\cos\left[2\pi\left(q_a+\frac{q_c}{2}\right)\right] + J_7\cos\left[2\pi\left(q_a-\frac{q_c}{2}\right)\right],$$
$$\Lambda_3(\boldsymbol{q}) = J_2\cos(\pi q_c) + J_8\cos\left[2\pi\left(q_a+\frac{q_c}{2}\right)\right] + J_9\cos\left[2\pi\left(q_a-\frac{q_c}{2}\right)\right]. \tag{12}$$

Now let us transform to magnetic normal coordinates

$$\begin{pmatrix}S_x(\boldsymbol{q},1)\\ S_x(\boldsymbol{q},2)\\ S_b(\boldsymbol{q},1)\\ S_b(\boldsymbol{q},2)\end{pmatrix} = \sigma_{+,x}(\boldsymbol{q})\boldsymbol{S}_{+,x}(\boldsymbol{q}) + \sigma_{-,x}(\boldsymbol{q})\boldsymbol{S}_{-,x}(\boldsymbol{q}) + \sigma_{+,b}(\boldsymbol{q})\boldsymbol{S}_{+,b}(\boldsymbol{q}) + \sigma_{-,b}(\boldsymbol{q})\boldsymbol{S}_{-,b}(\boldsymbol{q}). \tag{13}$$

Here, $\sigma_{+,x}(\boldsymbol{q})$, $\sigma_{-,x}(\boldsymbol{q})$, $\sigma_{+,b}(\boldsymbol{q})$, and $\sigma_{-,b}(\boldsymbol{q})$ are the magnetic order parameters for a magnetic structure with wave vector $\boldsymbol{q}$. The diagonal form of the magnetic free energy (6) is

therefore

$$f_{\rm mag} = \frac{1}{2}\sum_{\boldsymbol{q}}[\zeta_{+,x}(\boldsymbol{q},T)|\sigma_{+,x}(\boldsymbol{q})|^2 + \zeta_{-,x}(\boldsymbol{q},T)|\sigma_{-,x}(\boldsymbol{q})|^2 + \zeta_{+,b}(\boldsymbol{q},T)|\sigma_{+,b}(\boldsymbol{q})|^2 + \zeta_{-,b}(\boldsymbol{q},T)|\sigma_{-,b}(\boldsymbol{q})|^2] + O(\sigma^4). \quad (14)$$

At high enough temperatures, the eigenvalues (9) are all positive and therefore the stable phase is the paramagnetic one. As we lower the temperature, we reach a critical temperature for which one of the eigenvalues vanishes. We denote the wave vector for which one of the eigenvalues vanishes first as $\boldsymbol{q}_{\rm IC}$. Since $\lambda_+(\boldsymbol{q}) > \lambda_-(\boldsymbol{q})$ and $D > 0$, the first eigenvalue which reaches zero is $\zeta_{+,x}$. At the temperature $T_{N3}^{(0)}$ at which $\zeta_{+,x} = 0$, there is a phase transition from the paramagnetic phase to the AF3 phase, in which $\sigma_{+,x}(\boldsymbol{q}_{\rm IC}) \neq 0$, but all other order parameters remain zero. At the second transition AF3→AF2, the order parameter $\sigma_{+,b}(\boldsymbol{q}_{\rm IC})$ orders as well. This is true provided that

$$\lambda_+(\boldsymbol{q}_{\rm IC}) - \lambda_-(\boldsymbol{q}_{\rm IC}) > D. \quad (15)$$

The last condition ensures that $\zeta_{+,b}(\boldsymbol{q}_{\rm IC},T)$ vanishes before $\zeta_{-,x}(\boldsymbol{q}_{\rm IC},T)$ as the temperature is lowered. Henceforth, we will omit the plus sign in the order parameter's subscript.

To describe the electric polarization, we need to add an electric free energy and a magnetoelectric coupling term to the magnetic free energy. Assuming a homogeneous polarization, the expression for the electric free energy to lowest order is

$$f_{el} = V_{\rm cell}\sum_{\alpha=1}^{3}\frac{P_\alpha^{\,2}}{2\chi_{E,\alpha}^0}, \quad (16)$$

where $V_{\rm cell}$ is the volume of the unit cell, $\boldsymbol{P}$ is the ferroelectric order parameter, and $\chi_{E,\alpha}^0$ is the high-temperature electric susceptibility along the α direction. By symmetry considerations,[12] the allowed magnetoelectric coupling term of the lowest order in the incommensurate phases is

$$f_{\rm int} = r|\sigma_x(\boldsymbol{q}_{\rm IC})||\sigma_b(\boldsymbol{q}_{\rm IC})|\sin(\varphi_x - \varphi_b)P_b, \quad (17)$$

where φ_x and φ_b are the phases of $\sigma_x(\boldsymbol{q}_{\rm IC})$ and $\sigma_b(\boldsymbol{q}_{\rm IC})$, respectively, and r is a small real magnetoelectric coupling parameter. We emphasize that the form (17) of the magnetoelectric coupling follows from general symmetry considerations and does not necessarily follow from any specific microscopic model. Thus, it is not necessarily described by the spin-current[14] or by the inverse Dzyaloshinskii-Moriya[15] mechanisms. In fact, it has been shown in Ref. 31 that the ferroelectric polarization in $MnWO_4$ may be a result of purely symmetric exchange interactions. A similar conclusion has been derived in the context of the multiferroic $Ni_3V_2O_8$.[13] In the following, we examine the results of the model.

III. PHASE BOUNDARIES AND ORDER PARAMETERS

A. $MnWO_4$ without magnetic fields

The wave vector $\boldsymbol{q}_{\rm IC}$ that characterizes the AF3 and AF2 phases is determined by maximizing the eigenvalue $\lambda_+(\boldsymbol{q})$ for a given set of coupling energies $\{J_i\}$. After carrying out the maximization procedure, we can find the first transition temperature by equating $\zeta_{+,x}$ to zero for $\boldsymbol{q} = \boldsymbol{q}_{\rm IC}$:

$$T_{N3}^{(0)} = \frac{\lambda_+(\boldsymbol{q}_{\rm IC}) + D}{a}. \quad (18)$$

The index 0 indicates that this is the transition temperature in the absence of external magnetic fields. By transforming to normal magnetic coordinates, the free energy of the incommensurate phases up to the fourth order in the magnetic order parameters is

$$f = [aT - D - \lambda_+(\boldsymbol{q}_{\rm IC})]|\sigma_x(\boldsymbol{q}_{\rm IC})|^2 + 3b|\sigma_x(\boldsymbol{q}_{\rm IC})|^4 + [aT - \lambda_+(\boldsymbol{q}_{\rm IC})]|\sigma_b(\boldsymbol{q}_{\rm IC})|^2 + 3b|\sigma_b(\boldsymbol{q}_{\rm IC})|^4 + 2b|\sigma_x(\boldsymbol{q}_{\rm IC})|^2|\sigma_b(\boldsymbol{q}_{\rm IC})|^2[2 + \cos(2\varphi_x - 2\varphi_b)] + V_{\rm cell}\sum_{\alpha=1}^{3}\frac{P_\alpha^{\,2}}{2\chi_{E,\alpha}^0} + r|\sigma_x(\boldsymbol{q}_{\rm IC})||\sigma_b(\boldsymbol{q}_{\rm IC})|\sin(\varphi_x - \varphi_b)P_b. \quad (19)$$

This expression is obtained by keeping the Fourier components $\boldsymbol{q} = \pm\boldsymbol{q}_{\rm IC}$ in the total free energy $f = f_{\rm mag} + f_{el} + f_{\rm int}$. Minimizing with respect to the polarization components, we find the induced polarization

$$P_x = P_z = 0, \quad P_b = -\frac{\chi_{E,b}^0 r}{V_{\rm cell}}|\sigma_x(\boldsymbol{q}_{\rm IC})||\sigma_b(\boldsymbol{q}_{\rm IC})|\sin(\varphi_x - \varphi_b). \quad (20)$$

By inserting Eqs. (20) into (19), we get

$$f = [aT - D - \lambda_+(\boldsymbol{q}_{\rm IC})]|\sigma_x(\boldsymbol{q}_{\rm IC})|^2 + 3b|\sigma_x(\boldsymbol{q}_{\rm IC})|^4 + [aT - \lambda_+(\boldsymbol{q}_{\rm IC})]|\sigma_b(\boldsymbol{q}_{\rm IC})|^2 + 3b|\sigma_b(\boldsymbol{q}_{\rm IC})|^4 + 2b|\sigma_x(\boldsymbol{q}_{\rm IC})|^2|\sigma_b(\boldsymbol{q}_{\rm IC})|^2[2 + \cos(2\varphi_x - 2\varphi_b) - 2\gamma\sin^2(\varphi_x - \varphi_b)], \quad (21)$$

where γ is a dimensionless parameter given by

$$\gamma = \frac{\chi_{E,b}^0 r^2}{8V_{\rm cell}b}. \quad (22)$$

In order to minimize the free energy (21), the phase difference $\varphi_x - \varphi_b$ should be $\pm\pi/2$. In addition, we show in the following that γ is of order 10^{-5}. Hence, the last factor in the square brackets of Eq. (21) will be neglected in the description of the magnetic

phase transitions. The minimization of the free energy (21) with respect to $|\sigma_x(\boldsymbol{q}_{\rm IC})|$ and $|\sigma_b(\boldsymbol{q}_{\rm IC})|$ yields

$$|\sigma_x^0(\boldsymbol{q}_{\rm IC})| = \sqrt{\frac{a\left(T_{N3}^{(0)} - T\right)}{6b}}, \quad |\sigma_b^0(\boldsymbol{q}_{\rm IC})| = 0, \quad T_{N2}^{(0)} < T < T_{N3}^{(0)},$$
$$|\sigma_x^0(\boldsymbol{q}_{\rm IC})| = \sqrt{\frac{a\left(4T_{N3}^{(0)} - T_{N2}^{(0)} - 3T\right)}{24b}}, \quad |\sigma_b^0(\boldsymbol{q}_{\rm IC})| = \sqrt{\frac{a\left(T_{N2}^{(0)} - T\right)}{8b}}, \quad T < T_{N2}^{(0)}, \tag{23}$$

and the corresponding free energies are

$$f_{\rm AF3}^{(0)} = -\frac{a^2\left(T_{N3}^{(0)} - T\right)^2}{12b}, \quad T_{N2}^{(0)} < T < T_{N3}^{(0)},$$
$$f_{\rm AF2}^{(0)} = -\frac{a^2\left[4\left(T_{N3}^{(0)} - T\right)^2 + \frac{8}{3}\left(T - T_{N3}^{(0)}\right)\left(T_{N3}^{(0)} - T_{N2}^{(0)}\right) + \frac{4}{3}\left(T_{N3}^{(0)} - T_{N2}^{(0)}\right)^2\right]}{32b}, \quad T < T_{N2}^{(0)}, \tag{24}$$

with the transition temperature $T_{N2}^{(0)}$ given by

$$T_{N2}^{(0)} = T_{N3}^{(0)} - \frac{3D}{2a}. \tag{25}$$

By calculating the phase $\phi(\boldsymbol{q}_{\rm IC})$ of $J(\boldsymbol{q}_{\rm IC};\boldsymbol{\tau}_1,\boldsymbol{\tau}_2)$, we can find the magnetic structure of the phases AF3 and AF2. Using the experimental incommensurate wave vector $\boldsymbol{q}_{\rm IC} = (-0.214, 0.5, 0.457)$, this phase is found to be $\phi(\boldsymbol{q}_{\rm IC}) = 2\pi y$ for the two sets of exchange couplings. Using this relation and $\varphi_x - \varphi_b = \pm\pi/2$ in Eqs. (5) and (13), the spins of the two Mn^{2+} ions in the AF3 and AF2 phases are

$$\boldsymbol{S}(\boldsymbol{R} + \boldsymbol{\tau}_1) = \sqrt{2}\left|\sigma_x^0(\boldsymbol{q}_{\rm IC})\right| \cos(\boldsymbol{q}_{\rm IC}\cdot\boldsymbol{R} + \psi)\hat{\mathbf{x}} \mp \sqrt{2}\left|\sigma_b^0(\boldsymbol{q}_{\rm IC})\right| \sin(\boldsymbol{q}_{\rm IC}\cdot\boldsymbol{R} + \psi)\hat{\mathbf{b}}, \tag{26}$$

$$\boldsymbol{S}(\boldsymbol{R} + \boldsymbol{\tau}_2) = -\sqrt{2}\left|\sigma_x^0(\boldsymbol{q}_{\rm IC})\right| \cos(\boldsymbol{q}_{\rm IC}\cdot\boldsymbol{R} + \psi + \Delta\phi)\hat{\mathbf{x}} \pm \sqrt{2}\left|\sigma_b^0(\boldsymbol{q}_{\rm IC})\right| \sin(\boldsymbol{q}_{\rm IC}\cdot\boldsymbol{R} + \psi + \Delta\phi)\hat{\mathbf{b}}. \tag{27}$$

Here, ψ is an arbitrary phase and $\Delta\phi \equiv \boldsymbol{q}_{\rm IC}\cdot(\boldsymbol{\tau}_2 - \boldsymbol{\tau}_1) + \phi(\boldsymbol{q}_{\rm IC}) - \pi = \pi q_{{\rm IC},c}$, with $q_{{\rm IC},c}$ being the c component of $\boldsymbol{q}_{\rm IC}$. Using the experimental value $q_{{\rm IC},c} = 0.457$,[16] this phase is $\Delta\phi = 0.457\pi$. This is exactly the magnetic structure observed in neutron scattering studies.[16] We emphasize that while group theoretical analysis yields several magnetic structures consistent with the crystal symmetries, the magnetic structure described by Eqs. (26) is the actual structure observed in experiments. The two possible signs correspond to the phase difference $\varphi_x - \varphi_b = \pm\pi/2$ and represent spirals with opposite chirality:

$$\boldsymbol{S}(\boldsymbol{R} + \boldsymbol{\tau}_1) \times \boldsymbol{S}(\boldsymbol{R} + \boldsymbol{\tau}_2) = \pm 2\left|\sigma_x^0(\boldsymbol{q}_{\rm IC})\right|\left|\sigma_b^0(\boldsymbol{q}_{\rm IC})\right| \sin(\Delta\phi)\hat{\mathbf{z}}. \tag{28}$$

Here, $\hat{\mathbf{z}}$ is a unit vector perpendicular to the spiral plane. Various studies reveal that the spin chirality is strongly correlated with the electric polarization and can be controlled by poling the polarization with an external electric field.[32,33] This observation is in agreement with the form (20) of the electric polarization, in which $\varphi_x - \varphi_b$ changes sign together with $\boldsymbol{P}$.

Taking into account the magnetoelectric coupling in the description of the magnetic phase transitions will introduce small corrections to the transition temperature $T_{N2}^{(0)}$ and to the order parameters in the AF2 phase. As mentioned above, these corrections are governed by the dimensionless parameter γ [see Eq. (22)]. By using these corrections to the first order in γ, we find that the electric susceptibility takes the form

$$\chi_{E,b}(T) = \begin{cases} \chi_{E,b}^0 & T > T_{N3}^{(0)}, \\ \chi_{E,b}^0\left(1 + \frac{\widetilde{T}_{N2}^{(0)} - T_{N2}^{(0)}}{T - \widetilde{T}_{N2}^{(0)}}\right) & \widetilde{T}_{N2}^{(0)} < T < T_{N3}^{(0)}, \\ \chi_{E,b}^0\left(1 + g(T)\frac{\widetilde{T}_{N2}^{(0)} - T_{N2}^{(0)}}{\widetilde{T}_{N2}^{(0)} - T}\right) & T_{N1}^{(0)} < T < \widetilde{T}_{N2}^{(0)}, \\ \chi_{E,b}^0 & T < T_{N1}^{(0)}, \end{cases} \tag{29}$$

where $\widetilde{T}_{N2}^{(0)}$ is the shifted transition temperature:

$$\widetilde{T}_{N2}^{(0)} \approx T_{N2}^{(0)} + \gamma\left(T_{N3}^{(0)} - T_{N2}^{(0)}\right). \tag{30}$$

The function $g(T)$ is

$$g(T) = \frac{f_2(T)}{f_1(T)\left(T_{N3}^{(0)} - T_{N2}^{(0)}\right)} - 1, \tag{31}$$

where

$$f_1(T) = -8T + \frac{32}{3}T_{N3}^{(0)} - \frac{8}{3}T_{N2}^{(0)},$$
$$f_2(T) = 14T^2 + \nu_1 T + \nu_2, \tag{32}$$

with $\nu_1 = -\frac{1}{6}(95T_{N3}^{(0)} + 73T_{N2}^{(0)})$ and $\nu_2 = 16(T_{N3}^{(0)})^2 - \frac{97}{6}T_{N2}^{(0)}T_{N3}^{(0)} + \frac{85}{6}(T_{N2}^{(0)})^2$.

The first-order phase transition AF2→AF1 can be treated in the following way. Since the AF1 phase is characterized by the commensurate wave vectors $\boldsymbol{q}_{\rm C1,2} = (\pm\frac{1}{4}, \frac{1}{2}, \frac{1}{2})$, we calculate the free energy $f_{\rm AF1}^{(0)}$ for this phase and then look for a temperature below which $f_{\rm AF1}^{(0)} < f_{\rm AF2}^{(0)}$. Since $\boldsymbol{q}_{\rm C2} = -\boldsymbol{q}_{\rm C1} + (0,1,1)$, we need to consider only the Fourier components

$\boldsymbol{q} = \pm\boldsymbol{q}_C = \pm(\frac{1}{4},\frac{1}{2},\frac{1}{2})$ in Eq. (6). After some algebra, we find the free energy

$$f = [aT - D - \lambda_+(\boldsymbol{q}_C)]|\sigma_x(\boldsymbol{q}_C)|^2 + b|\sigma_x(\boldsymbol{q}_C)|^4[3+\cos(4\varphi - 4\pi y)]. \quad (33)$$

Here, φ is the phase of $\sigma_x(\boldsymbol{q}_C)$, determined to be $\pi(y+\frac{1}{4})$ in order to minimize the free energy. Therefore, the equilibrium order parameter and the corresponding free energy are

$$|\sigma_x(\boldsymbol{q}_C)| = \sqrt{\frac{\lambda_+(\boldsymbol{q}_C) + D - aT}{4b}}, \quad (34)$$

$$f^{(0)}_{AF1} = -\frac{[\lambda_+(\boldsymbol{q}_C) + D - aT]^2}{8b}. \quad (35)$$

For the commensurate wave vector $\boldsymbol{q}_C = (\frac{1}{4},\frac{1}{2},\frac{1}{2})$, we find the phase $\phi(\boldsymbol{q}_C) = 2\pi y - \pi$ of $J(\boldsymbol{q}_C;\boldsymbol{\tau}_1,\boldsymbol{\tau}_2)$ for both sets of exchange couplings. Using this relation and $\varphi = \pi(y+\frac{1}{4})$ in Eqs. (5) and (13), the spins of the two Mn^{2+} ions in the AF1 phase are

$$\begin{aligned}\boldsymbol{S}(\boldsymbol{R}+\boldsymbol{\tau}_1) &= \sqrt{2}|\sigma^0_x(\boldsymbol{q}_C)|\cos\left(\boldsymbol{q}_C\cdot\boldsymbol{R} + \frac{\pi}{4}\right)\hat{\mathbf{x}},\\ \boldsymbol{S}(\boldsymbol{R}+\boldsymbol{\tau}_2) &= -\sqrt{2}|\sigma^0_x(\boldsymbol{q}_C)|\cos\left(\boldsymbol{q}_C\cdot\boldsymbol{R} - \frac{\pi}{4}\right)\hat{\mathbf{x}}.\end{aligned} \quad (36)$$

Equations (36) describe a magnetic structure of the type $\uparrow\uparrow\downarrow\downarrow$ along both the a and c axes, in agreement with the structure observed in experiments.[16] We note again that this is the observed structure out of the two possible structures suggested by group theory.

The solution of the inequality $f^{(0)}_{AF1} < f^{(0)}_{AF2}$ is of the form $T < T^{(0)}_{N1}$ provided that

$$\epsilon > \max\left\{2(1-\eta), \frac{2}{3}(1-\sqrt{3\eta^2-2})\right\}, \quad (37)$$

where $\epsilon \equiv \frac{D}{\lambda_+(\boldsymbol{q}_{IC})}$ and $\eta \equiv \frac{\lambda_+(\boldsymbol{q}_C)}{\lambda_+(\boldsymbol{q}_{IC})}$. In this case, the transition temperature $T^{(0)}_{N1}$ is given by

$$T^{(0)}_{N1} = \left[\frac{4(\eta^2-1)+4\epsilon-3\epsilon^2}{4[2(\eta-1)+\epsilon]} + \epsilon\right]\frac{\lambda_+(\boldsymbol{q}_{IC})}{a}. \quad (38)$$

We study below the effects of magnetic field on the transition temperatures.

B. Effect of an external magnetic field

The formalism presented above can be generalized to take into account the effect of a uniform external magnetic field $\boldsymbol{h}$. This can be accomplished by adding to the free energy the Zeeman term $F_Z = g\mu_B\sum_{\boldsymbol{R}}\sum_{\boldsymbol{\tau}=\boldsymbol{\tau}_1,\boldsymbol{\tau}_2}\boldsymbol{S}(\boldsymbol{R}+\boldsymbol{\tau})\cdot\boldsymbol{h}$, or, equivalently,[34]

$$f_Z \equiv \frac{F_Z}{N} = g\mu_B\sum_{\boldsymbol{\tau}=\boldsymbol{\tau}_1,\boldsymbol{\tau}_2}\boldsymbol{S}(0,\boldsymbol{\tau})\cdot\boldsymbol{h}. \quad (39)$$

By minimizing the free energy with respect to $S_\alpha(0,\boldsymbol{\tau})$ at the paramagnetic phase, we find the response to the external magnetic field

$$S_\alpha(0,\boldsymbol{\tau}) = -\frac{\chi_\alpha(T)}{g\mu_B}h_\alpha \qquad (\alpha = x,b), \quad (40)$$

with the magnetic susceptibility following a Curie-Weiss law

$$\chi_\alpha(T) = \frac{(g\mu_B)^2}{aT - D_\alpha - 2\sum_{i=1}^{11}J_i}. \quad (41)$$

By comparing Eq. (41) with the general Curie-Weiss law[35]

$$\chi_\alpha(T) = \frac{\frac{(g\mu_B)^2J(J+1)}{3k_B}}{T-\theta_\alpha}, \quad (42)$$

we identify the parameter a introduced in the expansion of the entropy [see Eq. (2)] as

$$a = \frac{3k_B}{J(J+1)}. \quad (43)$$

For Mn^{2+} ions with $J = S = 5/2$, this parameter is $a_{Mn} = 0.343k_B$. The Curie-Weiss temperature is related to the exchange couplings and the anisotropy energy by

$$\theta_\alpha = \frac{J(J+1)}{3k_B}\left(D_\alpha + 2\sum_{i=1}^{11}J_i\right). \quad (44)$$

In the incommensurate phases AF3 and AF2, Eq. (40) is replaced by

$$S_\alpha(0,\boldsymbol{\tau}) = \frac{-\chi_\alpha(T)h_\alpha}{g\mu_B\left[1+\frac{d_{1\alpha}|\sigma^0_x(\boldsymbol{q}_{IC})|^2 + d_{2\alpha}|\sigma^0_b(\boldsymbol{q}_{IC})|^2}{a(T-\theta_\alpha)}\right]}, \quad (45)$$

where $d_{1x} = d_{2b} = 12b$ and $d_{2x} = d_{1b} = 4b$. The corresponding form in the AF1 phase is

$$S_\alpha(0,\boldsymbol{\tau}) = \frac{-\chi_\alpha(T)h_\alpha}{g\mu_B\left[1+\frac{e_\alpha|\sigma^0_x(\boldsymbol{q}_C)|^2}{a(T-\theta_\alpha)}\right]}, \quad (46)$$

with $e_x = 12b$ and $e_b = 4b$. The ferromagnetic Fourier component at $\boldsymbol{q} = 0$ couples to the incommensurate and commensurate wave vectors through the fourth-order term in Eq. (6). This coupling modifies the coefficients of the free-energy expansion and, consequently, the transition temperatures. In the presence of an external magnetic field, the first two transition temperatures are (to second order in the magnetic field)

$$T_{N3}(h_x) = T^{(0)}_{N3}\left[1 - 12\frac{b\chi_x^2(T^{(0)}_{N3})}{aT^{(0)}_{N3}(g\mu_B)^2}h_x^2\right], \quad \boldsymbol{h} = h_x\hat{\mathbf{x}}, \quad T_{N3}(h_b) = T^{(0)}_{N3}\left[1 - 4\frac{b\chi_b^2(T^{(0)}_{N3})}{aT^{(0)}_{N3}(g\mu_B)^2}h_b^2\right], \quad \boldsymbol{h} = h_b\hat{\mathbf{b}}, \quad (47)$$

$$T_{N2}(h_x) = T^{(0)}_{N2}, \quad \boldsymbol{h} = h_x\hat{\mathbf{x}}, \quad T_{N2}(h_b) = T^{(0)}_{N2}\left[1 - 16\kappa\frac{b\chi_b^2(T^{(0)}_{N2})}{a(g\mu_B)^2}h_b^2\right], \quad \boldsymbol{h} = h_b\hat{\mathbf{b}}, \quad (48)$$

with $\kappa = (\frac{1}{T_{N2}^{(0)}} + \frac{8}{3(T_{N2}^{(0)}-\theta_b)})$. For an external magnetic field along the easy-axis direction, the inequality which determines the stability range of the AF1 phase is

$$T < T_{N1}^{(0)} + \frac{8b}{2[\lambda_+(\boldsymbol{q}_C) - \lambda_+(\boldsymbol{q}_{IC})] + D}\left\{T - 3\frac{\lambda_+(\boldsymbol{q}_C)+D}{a} + 2T_{N3}^{(0)} + \frac{1}{T-\theta_x}\left[18\left(T - \frac{\lambda_+(\boldsymbol{q}_C)+D}{a}\right)^2 - 8\left(T_{N3}^{(0)} - T\right)^2\right]\right\}\left(\frac{\chi_x(T)}{g\mu_B}\right)^2 h_x^2, \tag{49}$$

while for a magnetic field along the b direction it is

$$T < T_{N1}^{(0)} - \frac{8b}{2[\lambda_+(\boldsymbol{q}_C) - \lambda_+(\boldsymbol{q}_{IC})] + D}\left\{T + \frac{\lambda_+(\boldsymbol{q}_C)+D}{a} - \frac{2}{3}\left(2T_{N2}^{(0)} + 2T_{N2}^{(0)}\right) - \frac{1}{T-\theta_b}\left[2\left(T - \frac{\lambda_+(\boldsymbol{q}_C)+D}{a}\right)^2 - 8\left(\frac{T_{N3}^{(0)} + 2T_{N2}^{(0)}}{3} - T\right)^2\right]\right\}\left(\frac{\chi_x(T)}{g\mu_B}\right)^2 h_b^2. \tag{50}$$

Equations (47)–(50) describe the T-H phase diagrams up to second order in h.

C. Effect of doping

We can gain insight on the effect of small concentrations of magnetic Fe^{2+} or nonmagnetic Zn^{2+} and Mg^{2+} ions at the Mn sites in the following way. Assuming that the orbital angular momentum is quenched, we set $J = S = 2$ in Eq. (43) and identify the parameter a [see Eq. (2)] for the Fe^{2+} ion as $a_{Fe} = 0.5k_B$. Using this value, we get

$$a(x) = a_{Mn}x + a_{Fe}(1-x), \tag{51}$$

where x is the Fe concentration. Since the exchange couplings of Fe-Fe and Fe-Mn pairs as well as the anisotropy energy for the Fe ion are not known, we assume a linear dependence of the quantities $\lambda_+(\boldsymbol{q}_{IC})$, D, and $\eta = \frac{\lambda_+(\boldsymbol{q}_C)}{\lambda_+(\boldsymbol{q}_{IC})}$ for small values of x:

$$\lambda_+[\boldsymbol{q}_{IC}(x),x] = \lambda_{+,IC}(0) + c_1 x, \quad D(x) = D(0) + c_2 x, \quad \eta(x) = \eta(0) + c_3 x. \tag{52}$$

We use the relations (52) in order to modify the expressions (18), (25), and (38) for the transition temperatures. Then, by expanding these expressions to first order in x and fitting to the slopes measured in experiments,[20] we are able to extract the values of c_1, c_2, and c_3. We neglect any changes in the parameter b.

For the case of the nonmagnetic Zn^{2+} ion, we set $a_{Zn} = D_{Zn} = 0$ as well as $J_i^{Zn-Mn} = J_i^{Zn-Zn} = 0$, and find the x dependence of the different parameters

$$\lambda_+(\boldsymbol{q},x) = \lambda_+(\boldsymbol{q})(1-x)^2, \quad a(x) = a(0)(1-x), \quad D(x) = D(0)(1-x), \quad \eta(x) = \eta(0). \tag{53}$$

Using these relations, the first two transition temperatures are given by

$$T_{N3}(x) = T_{N3}^{(0)} - \frac{\lambda_+(\boldsymbol{q}_{IC})}{a}x, \qquad T_{N2}(x) = T_{N2}^{(0)} - \frac{\lambda_+(\boldsymbol{q}_{IC})}{a}x. \tag{54}$$

These results explain the linear decrease of T_{N3} and of T_{N2} as a function of x observed in experiments.[24,25] The treatment of the AF2→AF1 transition is much more subtle and will be discussed below. We note that all the results above do not depend on the type of the nonmagnetic ion. This is in agreement with the observed similarities of the transition temperatures in Zn^{2+} and Mg^{2+} doping.[24,25]

IV. COMPARISON WITH EXPERIMENTS

In this section, we compare the results of the preceding section with different experimental observations and examine the consistency of the phase diagrams with the experimental sets of exchange couplings of Ehrenberg *et al.* and Ye *et al.* The results of the preceding section can be used to fit the parameters of the model within the Landau theory. We use Eqs. (18) and (25) with $a_{Mn} = 0.343k_B$ [see Eq. (43)] and the experimental transition temperatures $T_{N3}^{(0)}$ and $T_{N2}^{(0)}$ in order to extract the values of the parameters $\lambda_+(\boldsymbol{q}_{IC})$ and D for $MnWO_4$. Using the experimental values $T_{N3}^{(0)} \approx 13.5$ K and $T_{N2}^{(0)} \approx 12.3-12.7$ K, these parameters are found to be $\lambda_+(\boldsymbol{q}_{IC}) \approx 4.36-4.45$ K and $D = 0.27-0.18k_B$ K. The ratio $\eta = \frac{\lambda_+(\boldsymbol{q}_C)}{\lambda_+(\boldsymbol{q}_{IC})}$ is then chosen to be $\eta \approx 0.97-0.98$ in order to fit Eq. (38) to the experimental transition temperature $T_{N1}^{(0)} \approx 7-8$ K. These values are consistent with the condition (37).

Next we use Eqs. (42) and (47)–(50), with the experimental Curie-Weiss temperature $\theta_x \approx \theta_b \approx -75$ K,[17,36] and calculate the $T-H$ phase diagrams by fitting the parameter b. In order to get the best fit to the experimental phase diagram of Arkenbout *et al.*,[17] the parameter b was chosen to be $0.095k_B$ K. Figure 1 shows the results. The calculated and the experimental phase diagrams are in good agreement. Discrepancies at low temperatures or at high fields are expected due to the finite expansion of the free energy, which is terminated at fourth order. This means that the quantitative value of the ratio $\eta = \frac{\lambda_+(\boldsymbol{q}_C)}{\lambda_+(\boldsymbol{q}_{IC})}$, determined by the transition temperature $T_{N1}^{(0)}$ is less certain than the values of the parameters $\lambda_+(\boldsymbol{q}_{IC})$ and D, determined by the transition temperatures $T_{N3}^{(0)}$ and $T_{N2}^{(0)}$.

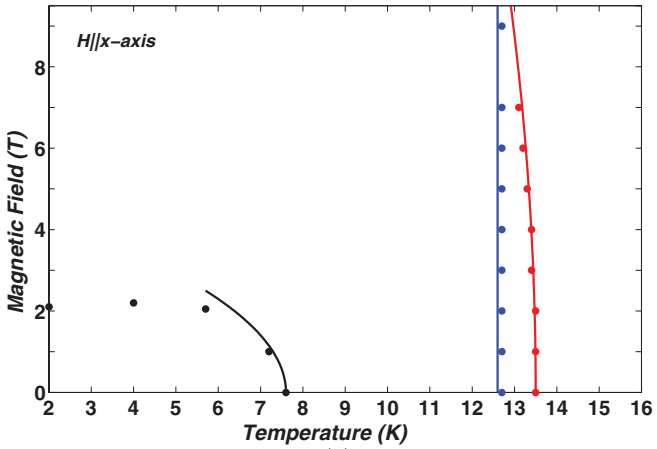

FIG. 1. (Color online) Magnetoelectric phase diagrams of $MnWO_4$ with magnetic fields parallel to the (a) easy and (b) b axes. The solid lines are the calculated transition temperatures and the dots describe the experimental points of Arkenbout *et al.* (Ref. 17). The calculated phase diagrams were obtained by setting $b = 0.095k_B$ K.

The development of the magnetic order parameters with decreasing temperature has been studied by polarized-neutron diffractions.[32] Generally, the magnetic moment at site $\boldsymbol{\tau}$ belonging to the unit cell at the lattice point $\boldsymbol{R}$ can be written as

$$\boldsymbol{m}(\boldsymbol{R}+\boldsymbol{\tau}) = m_x \cos(\boldsymbol{q}\cdot\boldsymbol{R}+\phi_\tau)\hat{\mathbf{x}} + m_b \sin(\boldsymbol{q}\cdot\boldsymbol{R}+\phi_\tau)\hat{\mathbf{b}}. \quad (55)$$

The cross sections for polarized-neutron scattering, where the neutrons are polarized parallel and antiparallel to the scattering vector, are given by[32]

$$I = I_0(m_x \pm m_b)^2, \quad (56)$$

with I_0 being a constant. Using Eqs. (26) and (36), we see that these cross sections are proportional to $(|\sigma_x^0(\boldsymbol{q}_{\rm IC})| \pm |\sigma_b^0(\boldsymbol{q}_{\rm IC})|)^2 + |\sigma_x^0(\boldsymbol{q}_{\rm C})|^2$. Then, from the second of Eqs. (23), the magnetic order parameters in the AF2 phase can be written as

$$|\sigma_x^0(\boldsymbol{q}_{\rm IC})| = \sqrt{\frac{a\left[\frac{4}{3}\left(T_{N3}^{(0)}-T_{N2}^{(0)}\right)+T_{N2}^{(0)}-T\right]}{8b}},$$
$$|\sigma_b^0(\boldsymbol{q}_{\rm IC})| = \sqrt{\frac{a\left(T_{N2}^{(0)}-T\right)}{8b}}. \quad (57)$$

Tolédano *et al.*[31] assumed that $|\sigma_x^0(\boldsymbol{q}_{\rm IC})|$ is fixed below $T_{N2}^{(0)}$. According to the first of Eqs. (57), such an assumption is valid only for $T_{N2}^{(0)} - T \ll \frac{4}{3}(T_{N3}^{(0)} - T_{N2}^{(0)})$. At lower temperatures, this assumption is inconsistent with the evolution of the observed integrated intensities reported in Ref. 32, which show that both $|\sigma_x^0(\boldsymbol{q}_{\rm IC})|$ and $|\sigma_b^0(\boldsymbol{q}_{\rm IC})|$ continue to grow below T_{N2}, with the ellipticity $p \equiv \frac{m_b}{m_x} = \frac{|\sigma_b^0(\boldsymbol{q}_{\rm IC})|}{|\sigma_x^0(\boldsymbol{q}_{\rm IC})|}$ approaching 1 (so that the spiral is almost circular) as the temperature decreases. Therefore, we preferred to use the explicit dependence of $|\sigma_x^0(\boldsymbol{q}_{\rm IC})|$ on the temperature. Using Eqs. (57), the ellipticity below T_{N2} can be written as

$$p = \frac{1}{\sqrt{1+\omega}}, \quad (58)$$

where $\omega \equiv \frac{4(T_{N3}^0 - T_{N2}^0)}{3(T_{N2}^0 - T)}$. Since the difference $T_{N3}^0 - T_{N2}^0 \approx 0.8$ K is very small in the case of $MnWO_4$, the ellipticity rapidly approaches 1 with decreasing temperature in the spiral phase AF2. The small difference $T_{N3}^0 - T_{N2}^0$ for $MnWO_4$ is a consequence of the small single-ion anisotropy of Mn^{2+} ions. This should be compared with the case of $TbMnO_3$, for which $T_{N3} \approx 42$ K and $T_{N2} \approx 27$ K. In this multiferroic, the ellipticity grows much more slowly with decreasing temperature[37] due to the large difference $T_{N3}^0 - T_{N2}^0 \approx 15$ K, which is in turn a result of the larger single-ion anisotropy of Mn^{3+} ions.[38] In Fig. 2, we sketch the quantities $(|\sigma_x^0(\boldsymbol{q}_{\rm IC})| \pm |\sigma_b^0(\boldsymbol{q}_{\rm IC})|)^2 + |\sigma_x^0(\boldsymbol{q}_{\rm C})|^2$ from Eqs. (57) and (34) together with the experimental data points of Ref. 32.

The development of the calculated order parameters is in a qualitative agreement with the temperature dependence of

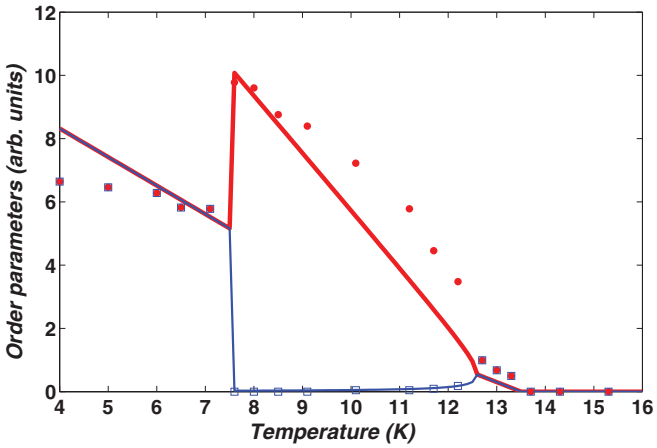

FIG. 2. (Color online) The temperature dependence of $(|\sigma_x^0(\boldsymbol{q}_{\rm IC})| \pm |\sigma_b^0(\boldsymbol{q}_{\rm IC})|)^2 + |\sigma_x^0(\boldsymbol{q}_{\rm C})|^2$. The red (thick) line corresponds to the plus sign and the blue (thin) one to the minus sign. The integrated intensities of the polarized-neutron diffraction (scaled by 0.002) from Ref. 32 are the red dots and the blue empty squares.

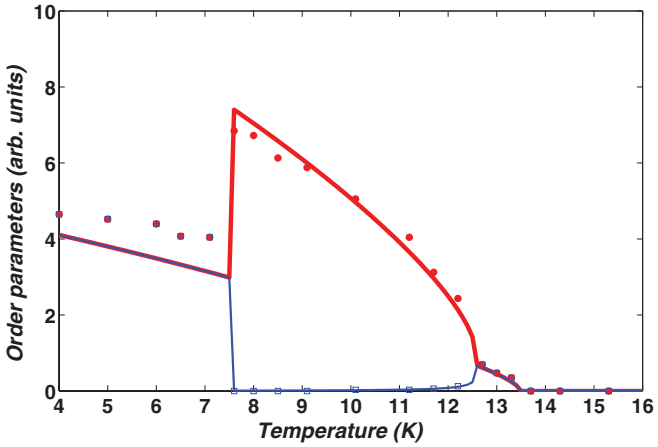

FIG. 3. (Color online) The temperature dependence of $(|\sigma_x^0(\boldsymbol{q}_{\rm IC})| \pm |\sigma_b^0(\boldsymbol{q}_{\rm IC})|)^2 + |\sigma_x^0(\boldsymbol{q}_{\rm C})|^2$ with the critical exponent $\beta \approx 1/3$. The red (thick) line corresponds to the plus sign and the blue (thin) one to the minus sign. The integrated intensities of the polarized-neutron diffraction (scaled by 0.0014) from Ref. 32 are the red dots and the blue empty squares.

the integrated intensities. However, for $T_{N2}^{(0)} - T \gg \frac{4}{3}(T_{N3}^{(0)} - T_{N2}^{(0)})$ in the AF2 phase, the quantity $(|\sigma_x^0(\boldsymbol{q}_{\rm IC})| + |\sigma_b^0(\boldsymbol{q}_{\rm IC})|)^2$ is linear in T, in contradiction with the temperature dependence of the integrated intensity, as can be seen in Fig. 2. A possible explanation for this apparent discrepancy is related to fluctuations near the transitions, which are not taken into account by the mean-field Landau theory.[39] As pointed out in Ref. 40, the transition P→AF3 belongs to the universality class of the XY model, while the transition AF3→AF2 belongs to the Ising universality class. Hence, we present in Fig. 3 the same quantities as in Fig. 2, but replacing the square roots of Eqs. (57) and (34) by the critical exponent $\beta = 1/3$, roughly appropriate for these two models. As seen from the figure, these revised expressions are in good agreement with the observed integrated intensities. This behavior illustrates the possible importance of fluctuations in $MnWO_4$. Further consequences of fluctuations near the transitions will be discussed below in the context of the Ginzburg criterion.

The magnetoelectric coupling r is determined by fitting Eq. (20) to the experimental data of the induced ferroelectric polarization.[18] The ferroelectric polarization is plotted in Fig. 4(a). The best fit to the experimental data is obtained for the value $\frac{\chi_{E,b}^0|r|}{V_{\rm cell}} = 21\mu C/m^2$. In addition, the electric susceptibility for $T > T_{N3}^{(0)}$ (in the paraelectric and paramagnetic phases) is experimentally found to be $\chi_{E,b}^0 = 11.3\epsilon_0$.[18] The dimensionless parameter γ [see Eq. (22)] is then $\gamma = 5.9 \times 10^{-5}$. This value supports the assumption that the magnetic transitions are almost unaffected by the magnetoelectric coupling. The dielectric constant $\epsilon_b = 1 + \frac{\chi_{E,b}^0}{\epsilon_0}$ is shown in Fig. 4(b). This result is in good agreement with the experimental measurements of Ref. 18. The narrow width of the divergence region is a consequence of the small difference between $\widetilde{T}_{N2}^{(0)}$ and $T_{N2}^{(0)}$. Once again, the discrepancy between the linear behavior of the calculated polarization and the observed one may be reconciled by assuming a critical exponent $\beta \approx \frac{1}{3}$ for the magnetic order parameters. The

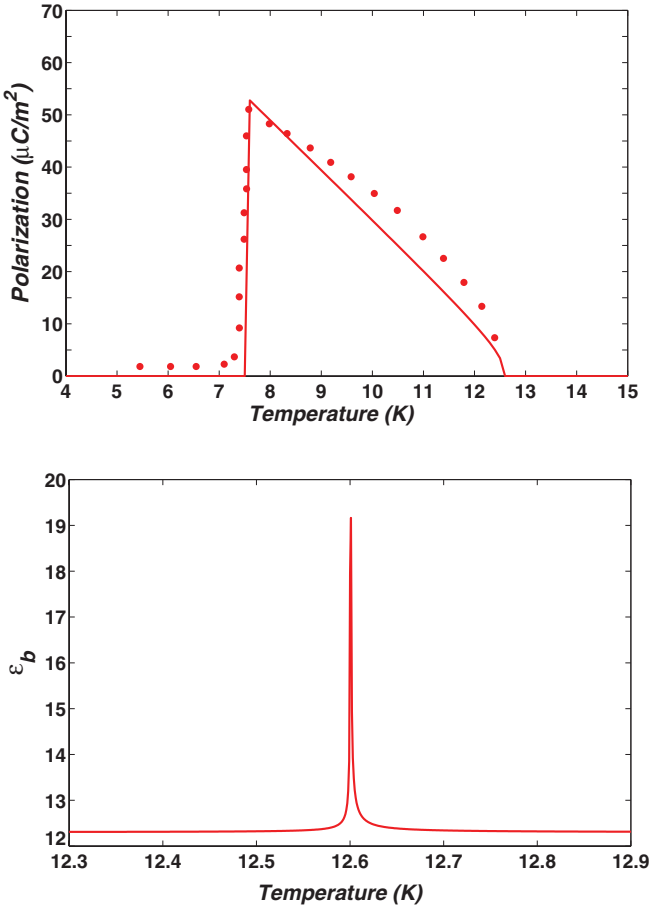

FIG. 4. (Color online) (a) The ferroelectric polarization and (b) the dielectric constant ϵ_b. The solid lines are the calculated quantities and the dots are the data points of Taniguchi *et al.* (Ref. 18). The calculated polarization was obtained by setting $\frac{\chi_{E,b}^0|r|}{V_{\rm cell}} = 21\mu C/m^2$.

behavior of the calculated polarization in this case is given in Fig. 5.

To examine the effect of Fe doping, we use the relations (51) and (52) in the expressions for the transition temperatures and fit the slope to the experimental value according to the $x-T$ phase diagram of Chaudhury *et al.*[20] This procedure yields the values $c_1 \approx -3.26k_B$ K, $c_2 \approx 13.03k_B$ K, and $c_3 \approx -1.3$. The anisotropy energy increases with increasing Fe concentration, as expected, since as opposed to the Mn^{2+} ion, the Fe^{2+} ion possesses a nonvanishing angular momentum.[41]

Calculating the different parameters for a small Fe concentration x and repeating the calculations of the $T-H$ phase diagram, we can check the consistency of the above results. The resulting phase diagram for $x = 0.035$ is shown in Fig. 6. Except for high fields or low temperatures, the result is in fine agreement with the measurement of Ye *et al.*[21] The reentrant ferroelectric phase observed at low temperatures[20,42] may be explained by higher-order terms in the free-energy expansion.

The effect of nonmagnetic ions on the transition temperatures $T_{N3}(x)$ and $T_{N2}(x)$ is given by Eq. (54). These results are drawn in Fig. 7 together with the experimental data of Chaudhury *et al.*[24] of $Mn_{1-x}Zn_xWO_4$. Similar results have been observed in $Mn_{1-x}Mg_xWO_4$.[25] We stress that unlike the

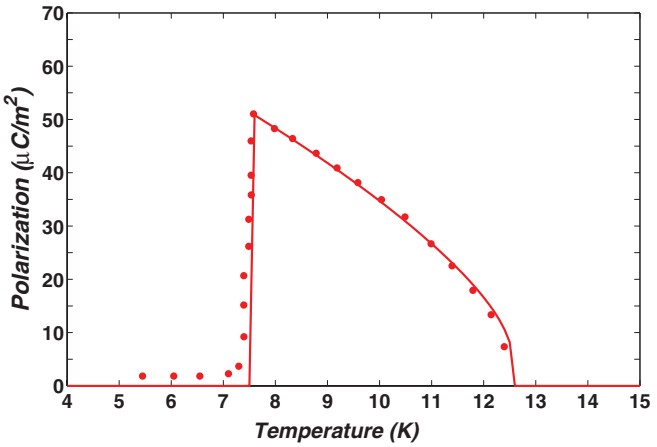

FIG. 5. (Color online) The ferroelectric polarization calculated with the critical exponent $\beta \approx \frac{1}{3}$. The solid lines are the calculated quantities and the dots are the experimental points of Taniguchi *et al*. (Ref. 18). The calculated polarization was obtained by setting $\frac{\chi^0_{E,b}|r|}{V_{\text{cell}}} = 27.5\mu C/m^2$.

case of Fe doping, the results for the transition temperatures $T_{N3}(x)$ and $T_{N2}(x)$ in the case of nonmagnetic ions doping do not require additional phenomenological parameters.

As opposed to $T_{N3}(x)$ and $T_{N2}(x)$, the calculated transition temperature $T_{N1}(x)$ does not coincide with the experimentally measured one.[24] The discrepancy may be explained by allowing small changes in the exchange couplings $J_i^{\text{Mn-Mn}}$ due to spin-lattice coupling (or exchange striction). In other words, if we assume that $J_i^{\text{Mn-Mn}}(x) = J_i^{\text{Mn-Mn}}(1 + \xi_i x)$ with $\xi_i x \ll 1$, then $T_{N1}(x)$ changes dramatically while $T_{N3}(x)$ and $T_{N2}(x)$ are almost not influenced. The reason for this behavior is that the transition temperature T_{N1} [see Eq. (38)] is much more sensitive to small changes in the exchange couplings than the transition temperatures T_{N3} and T_{N2} [see Eqs. (18) and (25)]. A significant spin-lattice coupling in the multiferroic $MnWO_4$ has been demonstrated[43] by the appearance of an incommensurate lattice modulation in the AF3 and AF2

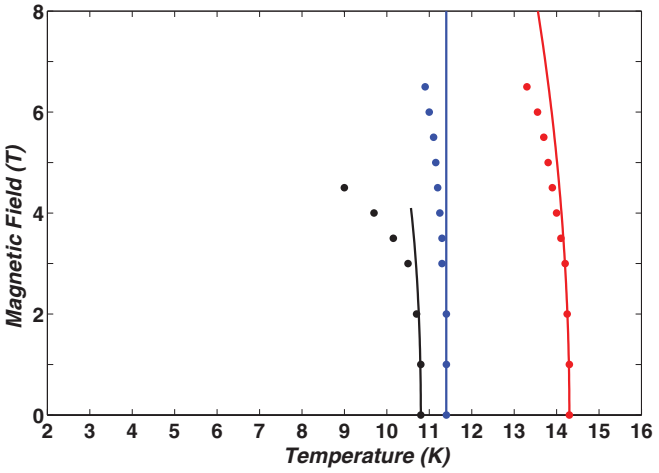

FIG. 6. (Color online) Magnetoelectric phase diagram of $Mn_{0.965}Fe_{0.035}WO_4$ with the magnetic field parallel to the easy axis. The solid lines are the calculated transition temperatures and the dots are the experimental points of Ye *et al*. (Ref. 21).

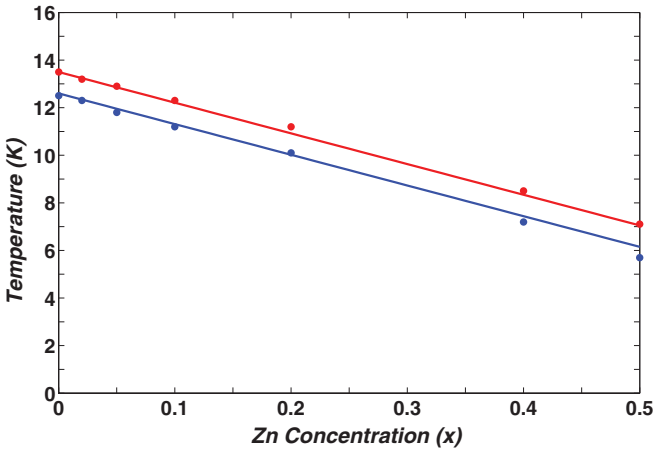

FIG. 7. (Color online) Transition temperatures $T_{N3}(x)$ and $T_{N2}(x)$ of $Mn_{1-x}Zn_xWO_4$. The solid lines are the calculated transition temperatures and the dots are the data points of Chaudhury *et al*. (Ref. 24).

phases, with a lattice propagation vector equal to twice the magnetic propagation vector. In addition, thermal expansion measurements reveal considerable discontinuities in the lattice parameters at the AF2→AF1 first-order phase transition.[44] Another indication for a dependence of the Mn-Mn exchange couplings on the nonmagnetic dopant concentration is provided by the small change of the incommensurate propagation vector from $\boldsymbol{q}_{\text{IC}} = (-0.214,0.5,0.457)$ in $MnWO_4$ to $\boldsymbol{q}_{\text{IC}} = (-0.209,0.5,0.453)$ in $Mn_{0.85}Zn_{0.15}WO_4$.[25]

The next step is to compare the above fitted parameters with the parameters calculated directly from the experimental sets of exchange couplings of Ehrenberg *et al*. and Ye *et al*. The calculated exchange couplings of Ref. 27 yield much higher transition temperatures than the observed ones and thus will not be discussed here. Indeed, the problem of overestimation of exchange interactions by DFT calculations has been indicated by the authors.[27]

The first step is to maximize $\lambda_+(\boldsymbol{q})$ [see Eq. (11)] in order to find the incommensurate wave vector $\boldsymbol{q}_{\text{IC}}$ and the corresponding eigenvalue $\lambda_+(\boldsymbol{q}_{\text{IC}})$. The maximization process yields $\boldsymbol{q}_{\text{IC}} = (-0.28,0.5,0.44)$ and $\lambda_+(\boldsymbol{q}_{\text{IC}}) = 3.82k_B$ K for the $J_1 - J_9$ values of Ehrenberg *et al*.,[26] while for the $J_1 - J_{11}$ values of Ye *et al*.,[28] we find $\boldsymbol{q}_{\text{IC}} = (-0.3,0.5,0.49)$ and $\lambda_+(\boldsymbol{q}_{\text{IC}}) = 3.85k_B$ K. For the exchange couplings of Ehrenberg *et al*. multiplied by a factor of 2 (second line in Table I), the wave vector $\boldsymbol{q}_{\text{IC}}$ remains $\boldsymbol{q}_{\text{IC}} = (-0.28,0.5,0.44)$ but now $\lambda_+(\boldsymbol{q}_{\text{IC}}) = 7.64k_B$ K. These results are in qualitative agreement with the incommensurate wave vector $\boldsymbol{q}_{\text{IC}} = (-0.214,\frac{1}{2},0.457)$ observed in experiments. However, the differences are not negligible, suggesting possible errors in the experimental sets of exchange couplings. We note that completely two different sets of exchange couplings yield almost the same wave vector $\boldsymbol{q}_{\text{IC}}$ and eigenvalue $\lambda_+(\boldsymbol{q}_{\text{IC}})$. This is a consequence of the form of $\lambda_+(\boldsymbol{q})$ [see Eqs. (11) and (12)] being a combination of 9 or 11 exchange couplings. This fact allows wide freedom in determining the exchange-couplings values, so that the same $\boldsymbol{q}_{\text{IC}}$ and $\lambda_+(\boldsymbol{q}_{\text{IC}})$ may be obtained from completely different sets. In addition, the transition temperatures $T_{N3}^{(0)}$ and $T_{N2}^{(0)}$ calculated

TABLE II. Comparison between the model parameters calculated from the experimental sets of Refs. 26 and 28 and those fitted to the experimental transition temperatures. The third column, denoted as Ref. 26*, refers to the couplings of Ref. 26 multiplied by a factor of 2.

Parameter	Ref. 26	Ref. 26*	Ref. 28	This work
$\lambda_+(\boldsymbol{q}_{\rm IC})(k_B\ {\rm K})$	3.82	7.64	3.85	4.36–4.45
$D(k_B\ {\rm K})$	0.568	0.568	0.83	0.27–0.18
η	0.974	0.974	0.97	0.97–0.98

from Eqs. (18) and (25) with $a_{\rm Mn} = 0.343k_B$ [see Eq. (43)] are found to be $T_{N3}^{(0)} = 12.79$ K, $T_{N2}^{(0)} = 10.3$ K for the set of Ehrenberg *et al.* and $T_{N3}^{(0)} = 13.67$ K, $T_{N2}^{(0)} = 10$ K for the set of Ye *et al.* These values slightly differ from the observed transition temperatures, especially the second one. However, for the set of Ehrenberg *et al.* multiplied by a factor of 2, the transition temperatures are $T_{N3}^{(0)} = 23.93$ K, $T_{N2}^{(0)} = 21.45$ K, both far above the observed transition temperatures. The ratio $\eta = \frac{\lambda_+(\boldsymbol{q}_{\rm C})}{\lambda_+(\boldsymbol{q}_{\rm IC})}$ is found to be $\eta = 0.974$ and 0.97 for the sets of Ehrenberg *et al.* (both the original and modified sets) and Ye *et al.*, respectively. Table II summarizes the values of $\lambda_+(\boldsymbol{q}_{\rm IC})$, D, and η calculated from the experimental sets of magnetic parameters and those fitted to the experimental transition temperatures.

The calculation of the Curie-Weiss temperature reveals a much more serious discrepancy. According to Eq. (44), the Curie-Weiss temperature is $\theta_x = -7.6$ K, $\theta_b = -9.25$ K for the set of Ehrenberg *et al.* and $\theta_x = -23.2$ K, $\theta_b = -25.65$ K for the set of Ye *et al.* The Curie-Weiss temperature for the set of Ehrenberg *et al.* multiplied by a factor of 2 is $\theta_x = -16.85$ K, $\theta_b = -18.5$ K. These values do not fit the experimental Curie-Weiss temperature $\theta \approx -75$ K.[17,36] We suspect that the origin of most of the discrepancies are errors in the set of magnetic couplings. The results suggested by our model may be used as additional constraints in the determination of those couplings. For instance, one may constrain the value of D to approximately $\approx 0.27{-}0.18k_B$ K, the value of $\lambda_+(\boldsymbol{q}_{\rm IC})$ to $\approx 4.36{-}4.45$ K, and the Curie-Weiss temperature in Eq. (44) to ≈ -75 K. Those constraints should reduce the wide freedom in determining the set of magnetic parameters from inelastic scattering measurements. As mentioned before, an additional possible cause for the above discrepancies is related to fluctuations near the transitions, as will be discussed in the next section.

V. GINZBURG CRITERION

The results of the preceding sections have been obtained within the mean-field approximation. Here, we estimate the Ginzburg range, in which fluctuations become important near the first transition P→AF3, by two methods. First, we compare the mean-square fluctuation of the order parameter $\sigma_x(\boldsymbol{q}_{\rm IC})$ with the mean-field value, and then we compare the discontinuity in the heat capacity derived from the Landau theory with the divergent heat capacity, originating from the fluctuations at quadratic order.[39]

Let us denote by $\delta\sigma_x(\boldsymbol{q}) = \sigma_x(\boldsymbol{q}) - \langle\sigma_x(\boldsymbol{q})\rangle$ the fluctuation of the order parameter in the AF3 phase. The correlation function of these deviations is

$$\langle\delta\sigma_x(\boldsymbol{q})\delta\sigma_x(\boldsymbol{q}')\rangle = \frac{k_BT\delta_{\boldsymbol{q}',-\boldsymbol{q}}}{4N[D+\lambda_+(\boldsymbol{q})-aT]}, \tag{59}$$

where N is the number of unit cells in the correlation volume. We can find the correlation lengths by expanding $\lambda_+(\boldsymbol{q})$ to second order around $\boldsymbol{q}_{\rm IC}$:

$$\lambda_+(\boldsymbol{q}) \approx \lambda_+(\boldsymbol{q}_{\rm IC}) + \sum_{i,j} M_{ij}(q_i - q_{{\rm IC},i})(q_j - q_{{\rm IC},j}), \tag{60}$$

with $M_{ij} \equiv \frac{1}{2}\frac{\partial^2\lambda_+(\boldsymbol{q})}{\partial q_i \partial q_j}|_{\boldsymbol{q}=\boldsymbol{q}_{\rm IC}}$. Denoting by μ_1, μ_2, and μ_3 the three eigenvalues of the positive matrix $-M_{ij}$, the three correlation lengths are

$$\xi_i = \sqrt{\frac{\mu_i}{a\left(T_{N3}^{(0)} - T\right)}}. \tag{61}$$

Substituting $\boldsymbol{q} = \boldsymbol{q}_{\rm IC}$ and $N = \frac{\xi_1\xi_2\xi_3}{V_{\rm cell}}$ in Eq. (59), the condition $\langle|\delta\sigma_x(\boldsymbol{q}_{\rm IC})|^2\rangle \ll |\sigma_x^0(\boldsymbol{q}_{\rm IC})|^2$ for the validity of the mean-field theory reads as[39]

$$\frac{k_BT_{N3}^{(0)}}{4a\left(T_{N3}^{(0)} - T\right)}\frac{V_{\rm cell}}{\xi_1\xi_2\xi_3} \ll \frac{a\left(T_{N3}^{(0)} - T\right)}{6b}. \tag{62}$$

By inserting Eq. (61) into (62) at the Ginzburg temperature T_G, we find

$$\left|T_G - T_{N3}^{(0)}\right| \approx \frac{9k_B^2b^2V_{\rm cell}^2\left(T_{N3}^{(0)}\right)^2}{4a\mu_1\mu_2\mu_3}. \tag{63}$$

Equation (63) estimates the temperature range below $T_{N3}^{(0)}$, in which fluctuations are not negligible.

Let us now estimate the Ginzburg range according to the second method. On the one hand, according to Landau theory, the heat capacity $c = -T\frac{\partial^2 f}{\partial T^2}$ grows discontinuously at the transition P→AF3:

$$\Delta c_L \equiv c_L\left(T_{N3}^{(0)-}\right) - c_L\left(T_{N3}^{(0)+}\right) = \frac{a^2T_{N3}^{(0)}}{6b}. \tag{64}$$

On the other hand, assuming fluctuations at quadratic order, the singular part of the heat capacity is given by

$$c_G = \frac{V_{\rm cell}k_Ba^2T^2}{2(2\pi)^3}\int_{\rm BZ}\frac{d^3q}{[aT - D - \lambda_+(\boldsymbol{q})]^2}, \tag{65}$$

where the integral is over the first Brillouin zone. In the neighborhood of $T_{N3}^{(0)}$, the main contribution to the integral comes from the neighborhood of the incommensurate wave vector $\boldsymbol{q}_{\rm IC}$ in reciprocal space. Thus, we can use the expansion (60). Replacing the first Brillouin zone by a sphere, and taking $T \approx T_{N3}^{(0)}$, we can estimate the integral in Eq. (65):

$$c_G \approx \frac{k_Ba^{1.5}T^2\left(T - T_{N3}^{(0)}\right)^{-0.5}}{16\pi\sqrt{\mu_1\mu_2\mu_3}}. \tag{66}$$

Comparing Eqs. (64) and (66) at the Ginzburg temperature T_G, we find[39]

$$\left|T_G - T_{N3}^{(0)}\right| \approx \left(\frac{6}{16\pi}\right)^2\frac{k_B^2b^2V_{\rm cell}^2\left(T_{N3}^{(0)}\right)^2}{a\mu_1\mu_2\mu_3}. \tag{67}$$

Calculating the eigenvalues μ_1, μ_2, and μ_3 from the experimental sets of exchange couplings, the Ginzburg temperature is estimated to be $|T_G - T_{N3}^{(0)}| \approx 9.41$ K and $|T_G - T_{N3}^{(0)}| \approx 6.24$ K for the sets of Ehrenberg *et al*. and Ye *et al*., respectively, by the first method [see Eq. (63)], while it is $|T_G - T_{N3}^{(0)}| \approx 0.06$ K and $|T_G - T_{N3}^{(0)}| \approx 0.04$ K by the second method [see Eq. (67)]. For the set of Ehrenberg *et al*. multiplied by a factor of 2, the Ginzburg temperature is $|T_G - T_{N3}^{(0)}| \approx 4.12$ K by the first method and $|T_G - T_{N3}^{(0)}| \approx 0.03$ K by the second method. These values suggest that fluctuations of the order parameters can also contribute to the discrepancies between the experimental data and the mean-field Landau theory results.

VI. SUMMARY AND CONCLUSIONS

We have studied the phase diagram of $Mn_{1-x}M_xWO_4$ (M = Fe, Zn, Mg) by a semiphenomenological Landau theory. The energy has been modeled by a Heisenberg Hamiltonian with a single-ion anisotropy, while the entropy has been expanded in powers of the classical spins. This approach is different from the previous theoretical studies,[31,45] which are purely phenomenological, since it enables us to compare different sets of exchange couplings. Although a purely phenomenological approach may capture all the symmetry aspects of the problem and may provide a full mapping of the stable states allowed by the order-parameter symmetries,[31] it does not indicate a clear connection between the free-energy coefficients and the microscopic interactions. The advantage of our approach is the simple relation of the free-energy coefficients with experimentally derived quantities such as the superexchange couplings and the anisotropy coefficients. For instance, this simple relation allows us to consider the effect of different dopants on the phase diagram, not discussed in Ref. 31. We emphasize that our approach does not contradict any symmetry requirement.

We used the superexchange interaction couplings from the inelastic neutron scattering studies of Ehrenberg *et al*.[26] and Ye *et al*.[28] Provided that the set of Ehrenberg *et al*. should not be multiplied by a factor of 2, the results show that both sets yield transition temperatures $T_{N3}^{(0)}$ and $T_{N2}^{(0)}$ that slightly deviate from the experimental temperatures, and significantly underestimate the Curie-Weiss temperature $|\theta|$. In addition, the calculated incommensurate wave vector $\boldsymbol{q}_{\rm IC}$ has non-negligible deviations from the experimentally observed one. However, if the set of Ehrenberg *et al*. should be multiplied by a factor of 2, then this set significantly overestimates the transition temperatures $T_{N3}^{(0)}$ and $T_{N2}^{(0)}$. In such case, the set of Ye *et al*. yields much better results. The results presented in this paper can serve as additional constraints on a future determination of the magnetic Hamiltonian parameters. Another possible cause for the discrepancies relates to fluctuations near the transitions. We have demonstrated the possible important contribution of fluctuations in $MnWO_4$. This issue should be further examined in future experiments.

Beyond that, the model clarifies the effect of different dopants on the phase diagram. The sensitivity of the expression (38) for the transition temperature $T_{N1}(x)$ to small changes of the ratio $\eta \equiv \frac{\lambda_+(\boldsymbol{q}_{\rm C})}{\lambda_+(\boldsymbol{q}_{\rm IC})}$ reflects the frustrated nature of the multiferroic $MnWO_4$. The origin of the complex phase diagram lies in the competition between different superexchange interactions. Small changes in the local environment of the Mn^{2+} ions due to a chemical doping cause a significant change in the phase diagram. The sensitivity for the local environment manifests itself by the contrasting behavior of doping with different ions.

Looking to the future, two points should be further examined. First, a new analysis of the inelastic scattering experiments, together with the additional constraints provided in this work, should improve the exchange couplings for the multiferroic $MnWO_4$. Second, the measurement of the critical exponents near the transitions would shed light on the effect of fluctuations. This may contribute to the general understanding of critical phenomena in multiferroics.

ACKNOWLEDGMENTS

We thank H. Shaked for helpful discussions. We acknowledge support from the Israel Science Foundation (ISF).

*Also at Tel Aviv University; aaharony@bgu.ac.il
†Also at Tel Aviv University.

[1] D. Khomskii, Physics **2**, 20 (2009).
[2] S.-W. Cheong and M. Mostovoy, Nat. Mater. **6**, 13 (2007).
[3] M. Fiebig, J. Phys. D: Appl. Phys. **38**, R123 (2005).
[4] T. Kimura, Annu. Rev. Mater. Res. **37**, 387 (2007).
[5] T. Kimura, T. Goto, H. Shintani, K. Ishizaka, T. Arima, and Y. Tokura, Nature (London) **426**, 55 (2003).
[6] N. Hur, S. Park, P. A. Sharma, J. S. Ahn, S. Guha, and S.-W. Cheong, Nature (London) **429**, 392 (2004).
[7] G. Lawes, A. B. Harris, T. Kimura, N. Rogado, R. J. Cava, A. Aharony, O. Entin-Wohlman, T. Yildrim, M. Kenzelmann, C. Broholm, and A. P. Ramirez, Phys. Rev. Lett. **95**, 087205 (2005).
[8] T. Kimura, J. C. Lashley, and A. P. Ramirez, Phys. Rev. B **73**, 220401(R) (2006).
[9] Y. Yamasaki, S. Miyasaka, Y. Kaneko, J.-P. He, T. Arima, and Y. Tokura, Phys. Rev. Lett. **96**, 207204 (2006).
[10] S. Picozzi and C. Ederer, J. Phys.: Condens. Matter **21**, 303201 (2009).
[11] M. Mostovoy, Phys. Rev. Lett. **96**, 067601 (2006).
[12] A. B. Harris, Phys. Rev. B **76**, 054447 (2007).
[13] A. B. Harris, T. Yildirim, A. Aharony, and O. Entin-Wohlman, Phys. Rev. B **73**, 184433 (2006).
[14] H. Katsura, N. Nagaosa, and A. V. Balatsky, Phys. Rev. Lett. **95**, 057205 (2005).
[15] I. A. Sergienko and E. Dagotto, Phys. Rev. B **73**, 094434 (2006).
[16] G. Lautenschläger, H. Weitzel, T. Vogt, R. Hock, A. Böhm, M. Bonnet, and H. Fuess, Phys. Rev. B **48**, 6087 (1993).
[17] A. H. Arkenbout, T. T. M. Palstra, T. Siegrist, and T. Kimura, Phys. Rev. B **74**, 184431 (2006).

[18]K. Taniguchi, N. Abe, T. Takenobu, Y. Iwasa, and T. Arima, Phys. Rev. Lett. **97**, 097203 (2006).
[19]H. Weitzel and H. Langhof, J. Magn. Magn. Mater. **4**, 265 (1977).
[20]R. P. Chaudhury, B. Lorenz, Y. Q. Wang, Y. Y. Sun, and C. W. Chu, New J. Phys. **11**, 033036 (2009).
[21]F. Ye, Y. Ren, J. A. Fernandez-Baca, H. A. Mook, J. W. Lynn, R. P. Chaudhury, Y.-Q. Wang, B. Lorenz, and C. W. Chu, Phys. Rev. B **78**, 193101 (2008).
[22]R. P. Chaudhury, B. Lorenz, Y. Q. Wang, Y. Y. Sun, and C. W. Chu, Phys. Rev. B **77**, 104406 (2008).
[23]Y.-S. Song, J.-H. Chung, J. M. S. Park, and Y.-N. Choi, Phys. Rev. B **79**, 224415 (2009).
[24]R. P. Chaudhury, F. Ye, J. A. Fernandez-Baca, B. Lorenz, Y. Q. Wang, Y. Y. Sun, H. A. Mook, and C. W. Chu, Phys. Rev. B **83**, 014401 (2011).
[25]L. Meddar, M. Josse, P. Deniard, C. La, G. André, F. Damay, V. Petricek, S. Jobic, M.-H. Whangbo, M. Maglione, and C. Payen, Chem. Mater. **21**, 5203 (2009).
[26]H. Ehrenberg, H. Weitzel, H. Fuess, and B. Hennion, J. Phys.: Condens. Matter **11**, 2649 (1999).
[27]C. Tian, C. Lee, H. Xiang, Y. Zhang, C. Payen, S. Jobic, and M.-H. Whangbo, Phys. Rev. B **80**, 104426 (2009).
[28]F. Ye, R. S. Fishman, J. A. Fernandez-Baca, A. A. Podlesnyak, G. Ehlers, H. A. Mook, Y. Wang, B. Lorenz, and C. W. Chu, Phys. Rev. B **83**, 140401(R) (2011).
[29]In a private communication with Dr. H. Ehrenberg, we have been informed that each pair in Ref. 26 was counted once, although the Heisenberg Hamiltonian in that paper was written as $H_{ex} = -\sum_{i\neq j} J_{ij}\boldsymbol{S}_i \cdot \boldsymbol{S}_j$. However, we also check the possibility of factor 2 between the two definitions of the exchange term.
[30]The values of the experimental parameters were adjusted to the definitions of Eq. (1), in which each pair of spins is counted once, and the anisotropy term includes a prefactor $\frac{1}{2}$.
[31]P. Tolédano, B. Mettout, W. Schranz, and G. Krexner, J. Phys.: Condens. Matter **22**, 065901 (2010).
[32]H. Sagayama, K. Taniguchi, N. Abe, T. H. Arima, M. Soda, M. Matsuura, and K. Hirota, Phys. Rev. B **77**, 220407(R) (2008).
[33]T. Finger, D. Senff, K. Schmalzl, W. Schmidt, L. P. Regnault, P. Becker, L. Bohatý, and M. Braden, Phys. Rev. B **81**, 054430 (2010).
[34]We note that Eq. (39) has a positive sign since the magnetic moment of electrons is opposite to the spin direction.
[35]N. W. Ashcroft and N. D. Mermin, *Solid State Physics* (Saunders, Philadelphia, 1976), Chap. 33.
[36]H. Dachs, Solid State Commun. **7**, 1015 (1969).
[37]Y. Yamasaki, H. Sagayama, T. Goto, M. Matsuura, K. Hirota, T. Arima, and Y. Tokura, Phys. Rev. Lett. **98**, 147204 (2007).
[38]The variation of the ellipticity with various parameters has been recently discussed for similar quantum spin models R. S. Fishman, Phys. Rev. B **84**, 052405 (2011); **85**, 024411 (2012).
[39]L. D. Landau and E. M. Lifshitz, *Statistical Physics* (Pergamon, London, 1958), Chap. XIV.
[40]A. B. Harris, A. Aharony, and O. Entin-Wohlman, J. Phys.: Condens. Matter **20**, 434202 (2008).
[41]N. Hollmann, Z. Hu, T. Willers, L. Bohatý, P. Becker, A. Tanaka, H. H. Hsieh, H.-J. Lin, C. T. Chen, and L. H. Tjeng, Phys. Rev. B **82**, 184429 (2010).
[42]R. P. Chaudhury, B. Lorenz, Y. Q. Wang, Y. Y. Sun, C. W. Chu, F. Ye, J. Fernandez-Baca, H. Mook, and J. Lynn, J. Appl. Phys. **105**, 07D913 (2009).
[43]K. Taniguchi, N. Abe, H. Sagayama, S. Otani, T. Takenobu, Y. Iwasa, and T. Arima, Phys. Rev. B **77**, 064408 (2008).
[44]R. P. Chaudhury, F. Yen, C. R. Dela Cruz, B. Lorenz, Y. Q. Wang, Y. Y. Sun, and C. W. Chu, Phys. B (Amsterdam) **403**, 1428 (2008).
[45]V. P. Sakhnenko and N. V. Ter-Oganessian, J. Phys.: Condens. Matter **22**, 226002 (2010).